



## Regular article

## Halogen optical referred pulse-compression thermography for defect detection of CFRP

Shichun Wu<sup>a</sup>, Bin Gao<sup>a,\*</sup>, Yang Yang<sup>b</sup>, Yuyu Zhu<sup>a</sup>, Pietro Burrascano<sup>c</sup>, Stefano Laureti<sup>c</sup>, Marco Ricci<sup>d</sup>, Yizhe Wang<sup>a</sup>

<sup>a</sup> School of Automation, University of Electronic Science and Technology of China, China

<sup>b</sup> Chengdu Aircraft Industry Co., Ltd, China

<sup>c</sup> Department of Engineering, University of Perugia, Polo Scientifico Didattico di Terni, Strada di Pentima 4, 05100 Terni, Italy

<sup>d</sup> Department of Informatics, Modeling, Electronics and System Engineering, University of Calabria, 87036 Rende, Italy



## ARTICLE INFO

## Keywords:

Carbon fiber reinforced polymer

Optical thermography

Pulse-compression

Halogen lamp

Non-destructive testing

## ABSTRACT

In this paper, pulse-compression thermography nondestructive testing method is proposed for defect detection in carbon fiber reinforced composite in reflection mode, using halogen lamps as excitation source. It is known that care should be taken when pulse-compression algorithm is applied to data obtained using halogen lamps. This because standard commercial halogen lamps suffer from high on/off switching delay time, thus they are not well-following the time behavior of the coded waveform employed for the heating emission modulation. The hereby-proposed method, named “Referred Pulse-Compression Thermography”, relies on subtracting the step heating contribution from the recorded coded thermal sequence before applying the pulse-compression algorithm. In particular, the step heating contribution is recorded separately by mean of an additional measurement. It is shown that the proposed method is inherently immune to the halogen-lamp switching time delay as both the reference recorded step signal and the coded signal sequence are affected by the same setback value. The proposed method can effectively enhance the defect information and improving the thermal contrast between defect and non-defect areas when halogen lamps are used in combination with pulse-compression in reflection mode. The validity of the proposed method is verified by experimental results and a comparison study with step heating thermography on different composite samples, having complex shapes and embedded artificial defects at different depths.

## 1. Introduction

Carbon fiber reinforced polymers (CFRPs) have many attracting features: light weight, high specific strength and modulus, dimensional stability, etc. [1–3]. Thanks to these characteristics, CFRP has become an indispensable structural material in the aircraft manufacturing industry [4,5]. However, quality issues in CFRP may be caused by cyclic stress, impact damages and any other anomaly buried within the composite structure. In fact, defects associated with composite materials (e.g. delamination, debonding, cracks and impact damage) will lead to a significant reduction of the load capacity and degradation of mechanical properties [6]. Therefore, it is necessary to conduct a reliable nondestructive testing (NDT) analysis to guarantee the safety [7].

In this framework, it must be noted that the detection of real defects in complex layered structures such as composites is more difficult than detecting artificially-realised defects in the same material or detecting

real defects in homogeneous materials. An example of such structure is the carbon fiber with honeycomb sandwich composite, which is commonly known as being difficult to be carefully inspected and evaluated.

In recent years, various NDT technologies have been proposed to evaluate the internal quality and assess structural integrity of CFRP structures. Examples of conventional methods of NDT include eddy current [8], ultrasonic testing [9], infrared thermography (IRT) [10], etc. Cawley [11] reviewed the available ultrasonic techniques and discussed the defect detection potential of lamb wave for composite laminates. Hsu et al. [12] discussed the principles of air coupled ultrasonic measurement, and then introduced several air-coupled ultrasonic non-destructive testing systems for composites. Lutz et al. [13] investigated the effect of the distance between the probe and the sample on the optimal range of measurement sensitivity. Koyama et al. [14] proposed a CP probe with a rectangular exciting coil in the upright position for defect detection in CFRP. In particular, the rapid

\* Corresponding author.

E-mail address: [bin.gao@uestc.edu.cn](mailto:bin.gao@uestc.edu.cn) (B. Gao).

<https://doi.org/10.1016/j.infrared.2019.103006>

Received 13 April 2019; Received in revised form 15 June 2019; Accepted 5 August 2019

Available online 07 August 2019

1350-4495/ © 2019 Elsevier B.V. All rights reserved.

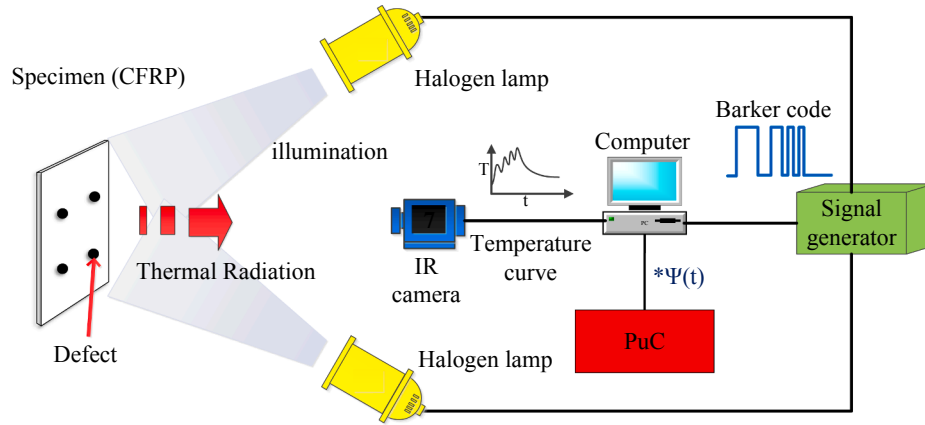


Fig. 1. Diagram of OPT system.

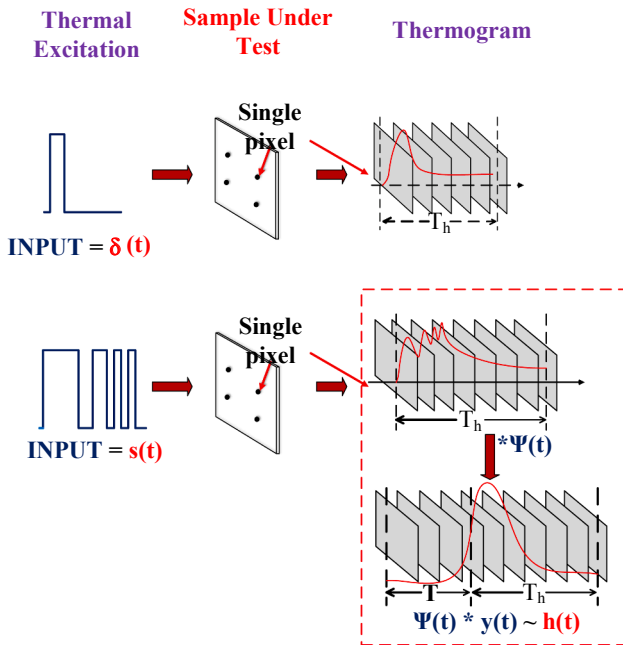


Fig. 2. Comparison of PT thermography and PuCT [57].

development of thermal image equipment is making IRT a quick and reliable NDT method [15]. IRT is in fact suitable for inspecting large areas having also complex geometries and it is applicable to different materials [16–18]. Compared with other nondestructive methods, IRT has many distinct advantages. These include rapid inspection over large areas, non-contact measurements and intuitive results interpretation. Examples of IRT application have been studied by many researchers, such as Cramer et al. [19], Bagavathiappan et al. [20], Doshvarpassand et al. [21], Laureti et al. [22–24]. Additionally, Sfarra et al. [25] detected the impacted laminates by using near-infrared reflectography and transmittography imaging, respectively. In active IRT schemes, different external excitation sources can be used such as optical lamp [26], microwave [27], ultrasonic [28], hot and cold air [29,30], eddy-current [31,32], etc. The use of external heat sources aims at provoking a thermal change onto/into the sample. It will result in a detectable thermal contrast among damaged and sound areas. In this framework, Optical Thermography (OT) is a subset of active IRT scheme whereby the heating is provided by optical sources - an example being halogen lamps or LED chips. OT is known to be an effective NDT scheme and has been extensively used for composite inspection. In OT, the detection rate and the Signal-to-Noise (SNR) are influenced by different parameters, e.g. source power, illumination angle, the distance between the

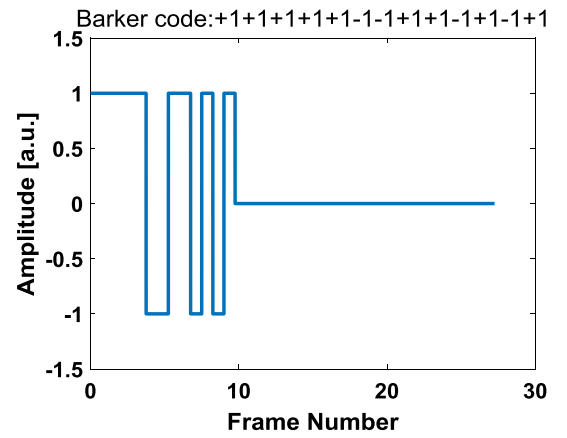


Fig. 3. 13-bit Barker code excitation used for driving the heat sources.

optical source and the inspected structure. To gain insight on the influence of the mentioned parameters, Chulkov et al. [33] compared three types of optical sources and found that the development of both hardware and software is required to improve the OT defect detection capability. As another example, Mabrouki et al. [34] investigated an aluminum-carbon fiber reinforced composite material and confirmed that small and deep defects can be detected by using a high-power optical source.

Commonly, OT is employed by using two main schemes: pulse thermography (PT) [35–40] and lock-in thermography (LIT) [41–43]. Several comparisons between PT and LIT can be found in literature [44,45]. With the fast-growing development of OT, concerning both the optimization of excitation sources for a given inspection and that of advanced post-processing algorithms, many types of defects within various composite types of structures have been successfully detected and characterized. However, there remain challenges in applying OT for the inspection of complex structure. Nevertheless, Pastuszak et al. [46] proved the effectiveness of PT for testing of curved composite structures by means of FEM simulation and experiment results. In addition, they found that the influence of the CFRP stacking order in the defect detection capability is negligible when PT is exploited. However, Alvarez-Restrepo et al. [47] obtained a limit for the inspection depth equal in value to 1.4 mm within several CFRP samples by using PT.

Recently, different methods have been developed to improve the detection capability in OT, attempting to combine the advantage of high SNR level for Lock-in Thermography (LIT) with the advantage of high number of information about the tested structure attainable for Pulse Thermography (PT). In this framework, Pulse-compression Thermography (PuCT) is an OT technique firstly introduced by Mulaveesala and Mandelis et al. [48–50].

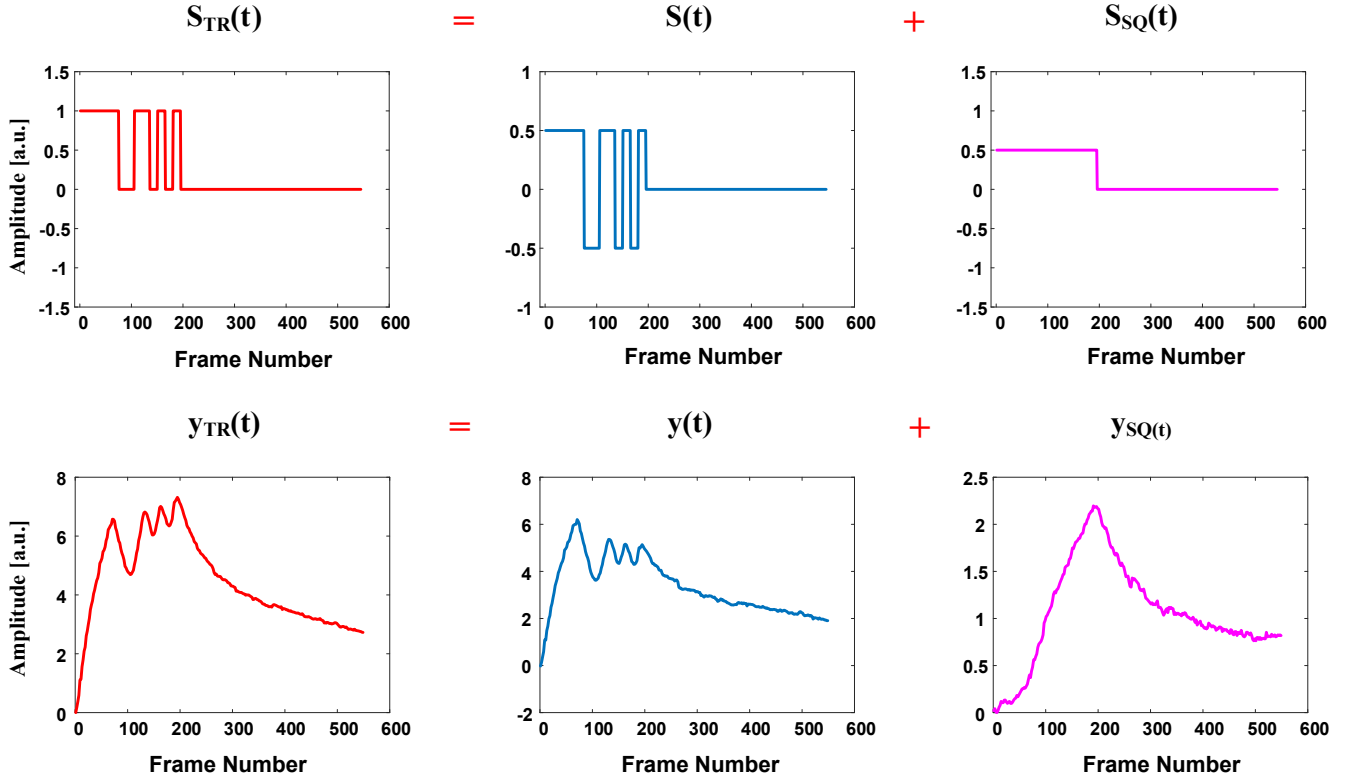


Fig. 4. Typical real input signal  $s_{TR}(t)$  and output signal  $y_{TR}(t)$  of PuCT method: input signal  $s_{TR}(t)$  is superimposed by coded excitation  $s(t)$  and step signal  $s_{SQ}(t)$ , and output signal  $y_{TR}(t)$  is superimposed by coded signal response  $y(t)$  and step heating [69–71] response  $y_{SQ}(t)$ .

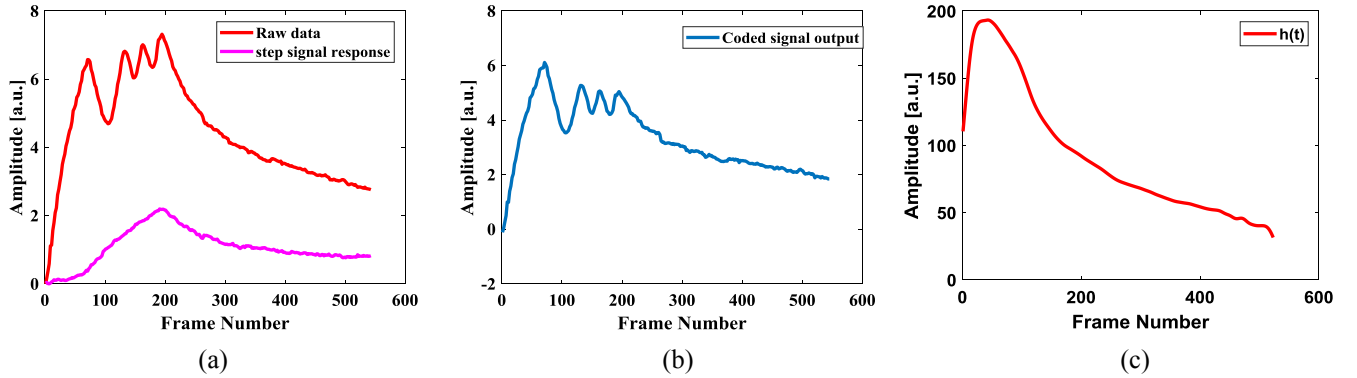


Fig. 5. Input signal response  $y_{TR}(t)$  and step heating response  $y_{SQ}(t)$  (a). The real coded signal output  $y(t)$  (b). The output signal  $h(t)$  after convolution (c).

PuCT is a correlation-based measurement, which extend to thermography the results obtained in many other NDT techniques. For instance, the Pulse-Compression (PuC) algorithm is extensively used in ultrasonic testing [51–53] and in photo-thermal analysis [54,55], the latter one being the closest example of application of PuC with respect to the PuCT. In PuCT, the heating stimulus is modulated via a coded signal such that its bandwidth and duration are almost independent. This characteristic is exploited to maximize the achievable SNR: the input is a long heating stimulus, e.g. comparable to LIT excitation, but with a bandwidth that cover the frequency range of interest for the inspection of the sample. A time-series of thermograms are collected during the excitation and for a certain time after its switch-off; this sequence is then properly correlated pixelwise with the input coded excitation. As a result, a new time-series of thermograms is obtained, which simulate the output of a short high-power excitation – as the one obtainable by PT – starting from the experimental data. The correlation step filters out the noise while enhancing the SNR in the output thermal sequence. In particular, the frequency and the duration of the coded

signal are chosen to be relevant to the type, thickness and depth of the material/defect to be investigated. In this framework Mulaveesala et al. [56] proposed a 7-bit barker coded excitation to improve the defect detectability in the obtained thermogram series after Pulse-Compression (PuC). Silipigni et al. [57] proposed an optimized PuCT excitation scheme to improve the SNR of defects. Other coded excitation strategies relying on the use of non-linear frequency modulated coded heating stimulus can be also found in literature [58,59].

So far, PuCT has been proved to be able to effectively improve the thermal contrast and enhance detection effect. Both halogen lamps or LED systems are commonly used to provide the heat stimulus. LED in the visible spectrum can operate at higher frequencies, thus allowing a better approximation of a PT experiment – in terms of both excited bandwidth and quality of the obtained impulse response – to be retrieved after the application of PuCT. Moreover, the excitation source spectrum is outside the sensitivity range of the IR cameras. The use of LED prevents collecting unwanted direct reflections of the source emission, which superimpose to the recorded signal. On the other hand,

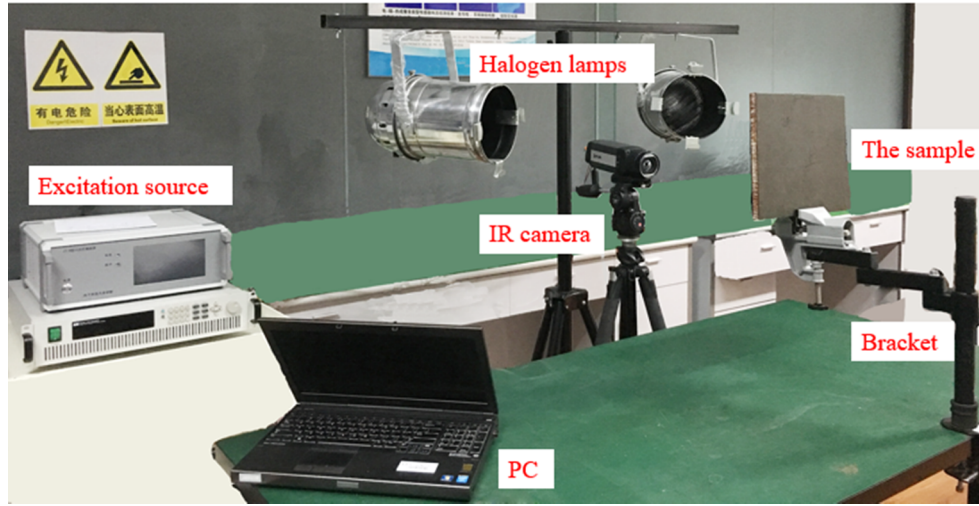


Fig. 6. The OT system.

LED chips have generally problems of low energy and are not suitable for some practical applications in the industrial field. Halogen lamps have instead higher heating power than LED chips. For this reason, halogen lamps were chosen as heat source in the present work where complex structures were to be inspected. However, due to the different process at the heart of the light generation, their modulation speed is significantly lower compared to LED chips, *i.e.* their intensity cannot be modulated as fast as in the LED case. In addition, the use of halogen lamps and PuCT requires either further post-processing steps or the employment of optical filters, as the IR reflection from the inspected sample is always captured by the IR cameras [60,61]. Moreover, the magnitude the IR reflection strictly depends on the nature of the investigated sample's surface and on choice of a transmission/reflection inspection mode. Regarding this last point, Meola [62] demonstrated that halogen lamps can be faithfully employed when used in transmission mode in OT. However, only a single side of the structure is often available in real life OT test, especially concerning the *in-situ* monitoring of aerospace composite parts. In addition, cumbersome setups associated with the employment of optical filters and extensive post-processing procedures should be avoided if a quick and repeatable test is aimed at being performed – this is especially the case of the aerospace industry. This fact indicates the importance of being able to use halogen lamps in combination with PuCT in a quick and easy way while fully exploiting the advantages of PuCT.

Some authors, see for example [63,64], have proposed to use the recorded signal from a sound area of the inspected sample as a way to improve the pulse-compression output quality. Conversely, this paper shows a new procedure for PuCT, called “Referred PuCT”, which shows promises to faithfully remove the step heating contribution due to the use of a monopolar heat source and to lower the effect of the slow switching time of halogen lamps. This in turns is reflected on the PuCT reconstructed thermograms, which can be interpreted without any further processing step. It is shown that the proposed method is inherently immune to the halogen-lamp switching time delay as both the reference recorded step signal and the coded signal sequence are affected by the same setback value. The mathematical theory at the base of the PuCT is analyzed, and then a reference experimental code strategy is proposed to overcome the delay problem of halogen lamp. A comparison between the proposed method with the traditional approach is carried out. In addition, different Barker Code excitations has been experimentally investigated.

The rest of the article is organized as follows. Section 2 introduces the methodology of OT and the optimized PuCT method. Section III describes the investigated samples and experimental setup. The experiment results and analysis are discussed in Section 4. Finally, Section

5 reports conclusions and perspectives of further developments.

## 2. Methodology

### 2.1. Pulse-compression thermography

In standard PT, the heating time is significantly shorter than the cooling time, *i.e.* of the typical times of thermal diffusion phenomena in the sample, so that it can be modeled as a Dirac's Delta function  $\delta(t)$ . If the linearity and time-invariance conditions hold, then the impulse response  $h(t, i, j)$  of the pixel  $(i, j)$  can be retrieved by just collecting a sequence of thermograms at different  $t$ -sampling values by means of a suitable IR camera. In fact, the excitation can be considered instantaneous and the sample impulse response is measured for a time  $T_h$ , which is large enough to record the main internal thermal diffusion process. The estimated impulse response can be expressed as Eq. (1):

$$h_{PT}(t, i, j) \sim h(t, i, j) + e(t, i, j) \quad (1)$$

where  $e(t, i, j)$  represents the environmental and instrumental noise, which is assumed as Additive White Gaussian Noise (AWGN).

Features of interest such as the presence of flaws/inclusion can be inferred from the analysis of the  $h_{PT}(t)$ 's cooling time. However, PT is not the only possible way to measure or estimate the thermal impulse response. Indeed, Pulse-Compression (PuC) is a well-established and effective measurement method used to estimate the impulse response of a Linear Time Invariant (LTI) system in a high noisy environment or with low SNR value. Fig. 1 shows the diagram of the PuCT system stimulated by two halogen lamps. The excitation signal is generated by a signal generator. The IR camera records synchronously to the excitation signal the temperature variation on the specimen and continue the acquisition for  $T_h$  second after the end of the excitation.

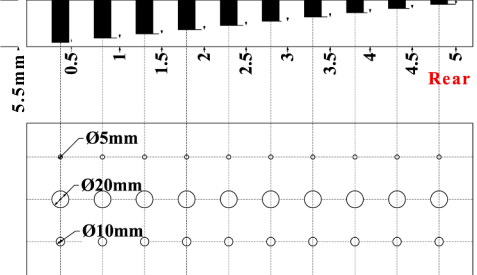

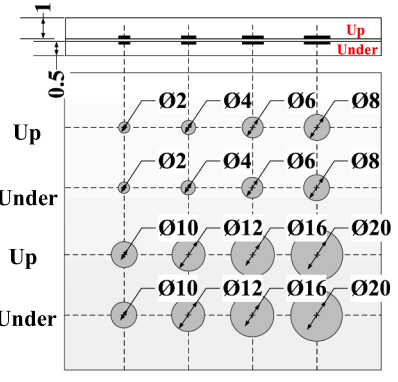
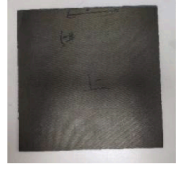
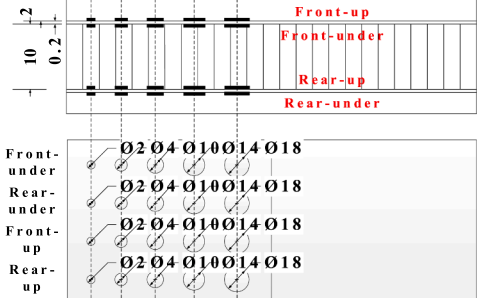

In particular, the sample is stimulated by a coded excitation  $s(t)$  of duration  $T$ ; thus, the total time interval of acquisition is  $T + T_h$ . The acquired thermograms are convolved pixel-by-pixel with the matched filter  $\psi(t)$ .  $\psi(t)$  is designed so that its convolution with the coded excitation  $s(t)$  approximates the Dirac's Delta function [57]:

$$s(t) * \psi(t) = \delta_{PuCT}(t) \approx \delta(t) \quad (2)$$

where “\*” denotes the convolution operation. The PuCT response of the pixel  $(i, j)$ ,  $h_{PuCT}(t, i, j)$  is then retrieved by convolving the system output  $y(t)$  with  $\psi(t)$ , as shown in Fig. 2.  $h_{PuCT}(t, i, j)$  is an estimation of the true impulse response of the sample  $h(t, i, j)$ : the closer is the approximation  $\delta_{PuCT}(t) \approx \delta(t)$ , the more accurate is the estimation.

The drawback of PuCT is that  $\delta_{PuCT}(t)$  is affected by the so-called sidelobes that represent a mathematical noise affecting the fidelity of

**Table 1**  
Description of specimens.

Specimen	Indication	Dimension (mm)	Defect information (mm)	Picture
SP1		530× 180× 5.5	Depth: 0.5, 1, 1.5, 2, 2.5, 3, 3.5, 4, 4.5, 5 Diameter: 5, 20, 10	
SP2		250× 250× 2.2	Depth: 1 or 1.2 Diameter: 2, 4, 6, 8, 10, 12, 16, 20	
SP3		250× 600× 27	Depth: 2, 2.2, 12.2, 12.4 Diameter: 3, 6, 10, 14, 18	

the impulse response reconstruction, so many efforts were devoted in PuC literature to reduce sidelobes by proper designing the matched filter  $\psi(t)$  [57–59,65–66]. The advantage of PuCT is that is possible to significantly reduce the noise in the  $h_{PuCT}(t, i, j)$  even with using low-power excitations that can be useful or mandatory in various cases [57].

To have an insight about the PuCT method, let us consider indeed the effect of the environmental and instrumentation noise on the procedure: the output time-trend of the pixel  $(i, j)$ ,  $y(t)$ , is described by  $y(t, i, j) = h(t, i, j) * s(t) + e(t, i, j)$  in which, as before,  $e(t, i, j)$  is Additive White Gaussian Noise.

The PuCT output  $h_{PuCT}(t, i, j)$  is expressed as Eq. (3):

$$h_{PuCT}(t, i, j) = y(t, i, j) * \psi(t) \quad (3)$$

Considering the definition of the output, the previous expression can be rewritten as [57]:

$$h_{PuCT}(t, i, j) = h(t, i, j) * s(t) * \Psi(t) + e(t, i, j) * \Psi(t) \quad (4)$$

By using Eq. (2), Eq. (3) becomes:

$$\begin{aligned} h_{PuCT}(t, i, j) &= h(t, i, j) * \delta_{PuCT}(t) + \tilde{e}(t, i, j) \approx h(t, i, j) * \delta(t) + \tilde{e}(t, i, j) \\ &= h(t, i, j) + \tilde{e}(t, i, j) \end{aligned} \quad (5)$$

Being the matched filter uncorrelated with  $e(t)$ , after pulse-compression  $\tilde{e}(t)$  is lower than  $e(t)$  leading to an increased SNR. The proposed method can therefore improve the detection resolution and thermal contrast effectively.

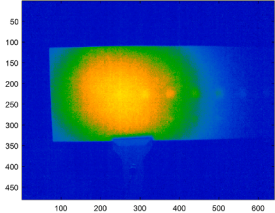
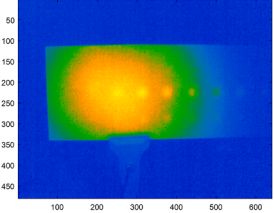
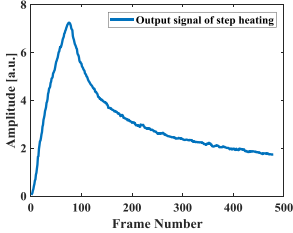
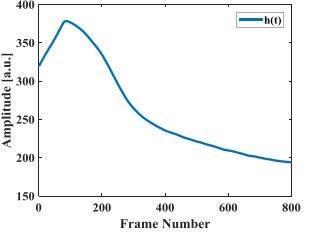
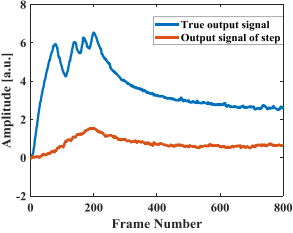
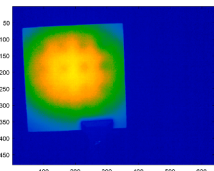
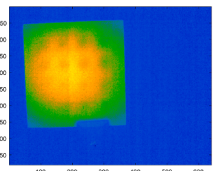
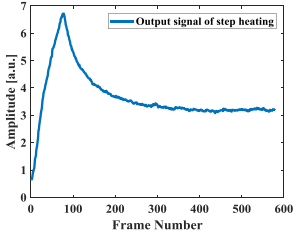
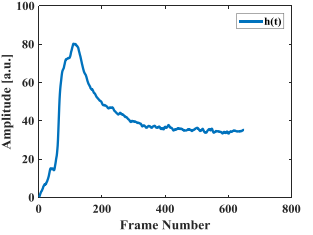
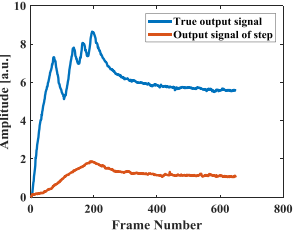
Different signal and matched filter can be investigated. Barker code is a kind of binary phase-modulated coded signal that is well-known to have the best self-correlation characteristic when used in aperiodic/single-shot mode [65] and the longest Barker code (13-bit) was selected to drive the heat sources. For this code, the peak value of the  $\delta_{PuCT}(t)$  main lobe is 13 times of the peak value of the side lobes. The signal is as shown in Fig. 3.

The auto-correlation function of Barker code sequence is defined as Eq. (6):



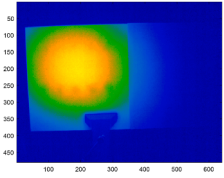
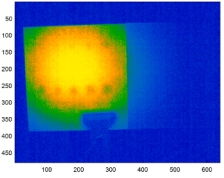
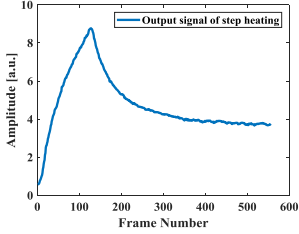
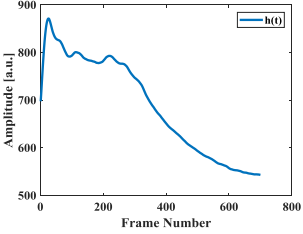
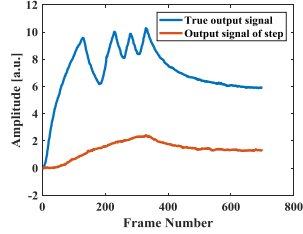
**Table 2**

The results obtained with step (left) and PuCT (right) methods for the three samples.

 <p>Best thermal image of SP1 obtained by step heating thermography</p>	 <p>Best thermal image of SP1 obtained by PuCT</p>	
 <p>The output signal of SP1 step heating thermography</p>	 <p>The coded output signal of SP1</p>	 <p>The true output signal and the step heating thermography of SP1</p>
(a) The result of SP1 with step heating thermography	(d) The result of SP1 with PuCT	
 <p>Best thermal image of SP2 obtained by step heating thermography</p>	 <p>Best thermal image of SP2 obtained by PuCT</p>	
 <p>The output signal of SP2</p>	 <p>The coded output signal of SP2</p>	 <p>The true output signal and the step heating thermography of SP2</p>
(b) The result of SP2 with step heating thermography	(e) The result of SP2 with PuCT	

(continued on next page)

Table 2 (continued)

 <p>Best thermal image of SP3 obtained by step heating thermography</p>	 <p>Best thermal image of SP3 obtained by PuCT</p>
 <p>The output signal of SP3</p>	 <p>The coded output signal of SP3</p>  <p>The true output signal and the step heating thermography of SP3</p>
(c) The result of SP3 with step heating thermography	(f) The result of SP3 with PuCT

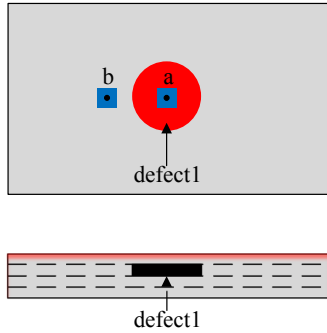


Fig. 7. Defect and background region definition.

$$R(j) = \sum_{i=1}^{N-j} X_i X_{i+j} = \begin{cases} n, & j = 0 \\ 0 \text{ or } \pm 1, & 0 < j < n \\ 0, & j \geq n \end{cases} \quad (6)$$

where  $N$  represents the code length of the barker code.

## 2.2. The proposed referred de-level method

When using pulse-compression in infrared OT, one of the main practical issues to face is the lack of a bipolar optical heat excitation, although the use of a cooling source has been recently reported [67]. The common heat sources used in infrared thermography are indeed unipolar, *i.e.* only capable of heating the sample. Therefore, it is not possible to apply directly bipolar excitation to the sample [68]. However, by exploiting the superposition principle and assuming the system to be linear, is still possible to implement PuCT even by using unipolar sources. The role of superposition principle in PuCT is shown in Fig. 4:

the true input unipolar signal  $s_{TR}(t) = s(t) + s_{SQ}(t)$  is a combination of the coded bipolar signal  $s(t)$  and of a step signal  $s_{SQ}(t)$ .

According to the superposition principle, the output  $y_{TR}(t) = s_{TR}(t) * h(t) + e(t)$  is a superposition of the coded signal output  $y(t)$  and of the output  $y_{SQ}(t) = s_{SQ}(t) * h(t)$  of the sole step signal  $s_{SQ}(t)$ . In order to correctly implement pulse-compression, the step heating response  $y_{SQ}(t)$  has therefore to be removed from the measured output  $y_{TR}(t)$ . In literature, various fitting function were proposed to remove the rising part of  $y_{SQ}(t)$ , typically with a linear or a polynomial fitting. However, in [44] it was showed that the correct implementation of the pulse-compression algorithm requires collecting data also when the excitation is switched off. This makes the fitting more challenging, and this is further hampered by the delayed response of halogen lamps with respect the driving voltage. A new method for removing the heating trend biasing the coded excitation output is here proposed to improve the quality of PuCT output.

The idea behind the underlying method is the following: the true coded signal output is given by  $y(t) = y_{TR}(t) - y_{SQ}(t)$ , as shown in Fig. 5. Fig. 5(a) represents the real input signal output  $y_{TR}(t)$  and  $y_{SQ}(t)$ , Fig. 5(b) represents the real coded signal output and Fig. 5(c) represents the output signal  $h(t)$  after convolution. So, if  $y_{SQ}(t)$  can be directly measured by using just a step signal excitation, then  $y(t)$  is retrieved by subtracting two measured thermal sequences. Of course, this require doing two separate measurements, *i.e.* doubling the measurement time, but the advantages in terms of defect detection can counterbalance the disadvantage of the additional measurement, especially in cases where with standard methods defects are not visible. In addition, since both step signal and coded unipolar signal suffer from the same halogen-lamp delay, the method is inherently immune to such problem. After subtracting the two measured sequences, the final PuCT output signal is then obtained by convolving the coded excitation response with the matched filter.

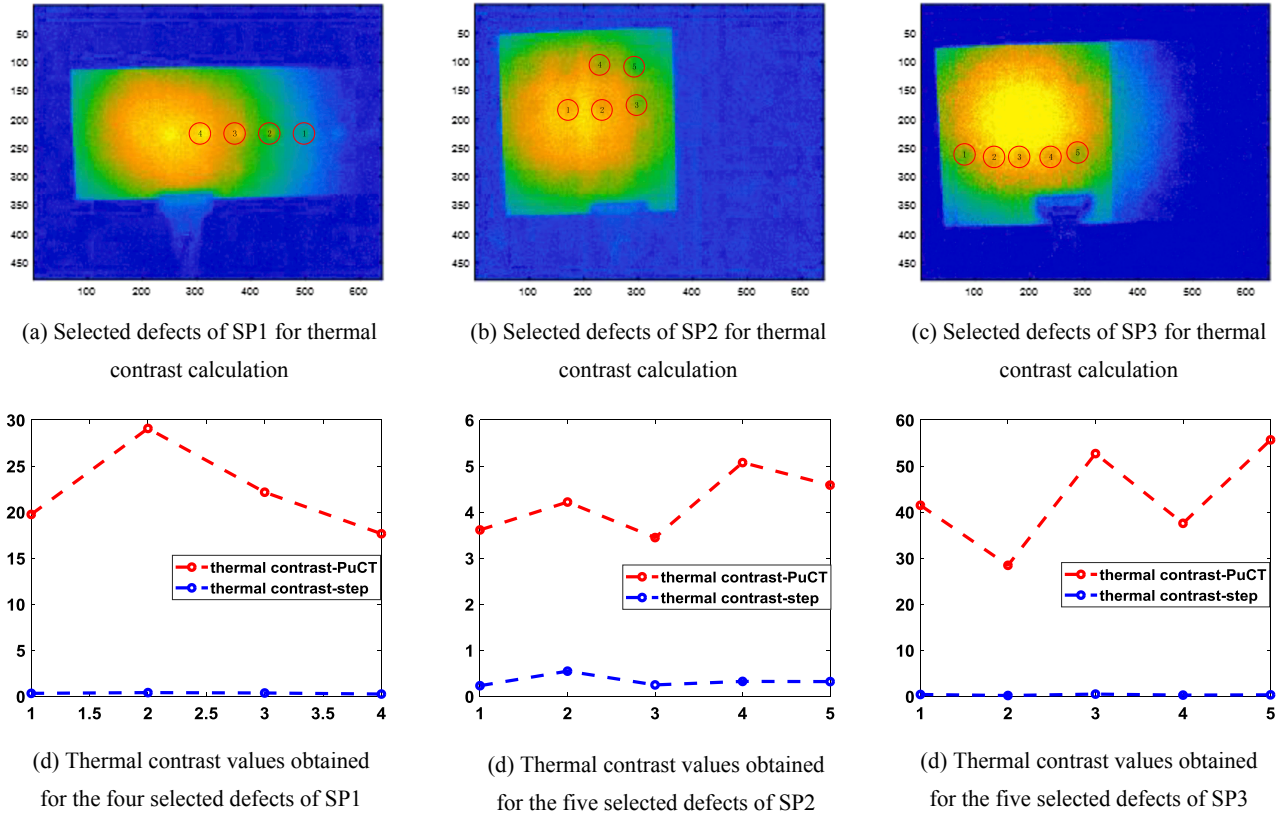


Fig. 8. The thermal contrast of three specimens acquired by the step heating thermography and the PuCT method.

Table 3

Difference in the thermal contrast values among PuCT and step heating results for the selected defects.

Specimen	Defect1	Defect2	Defect3	Defect4	Defect5	Average
SP1	19.42	28.67	21.79	17.40	None	21.82
SP2	3.38	3.67	3.19	4.75	4.26	3.85
SP3	41.07	28.25	52.20	37.29	55.34	42.83

Table 4

The thermal contrast of referred PuCT method and Step Heating.

Specimen	Method	Defect1	Defect2	Defect3	Defect4	Defect5
SP1	Referred PuCT	19.74	29.07	22.15	17.65	None
	Step Heating	0.32	0.40	0.36	0.25	None
SP2	Referred PuCT	3.61	4.21	3.44	5.07	4.58
	Step Heating	0.23	0.54	0.25	0.32	0.32
SP3	Referred PuCT	41.47	28.44	52.69	37.56	55.67
	Step Heating	0.40	0.19	0.49	0.27	0.33

Table 5

The SNR of referred PuCT method and Step Heating.

Specimen	Method	Defect1	Defect2	Defect3	Defect4	Defect5
SP1	Referred PuCT	4.82	4.24	5.19	4.66	None
	Step Heating	3.98	4.27	4.91	3.30	None
SP2	Referred PuCT	3.40	2.18	2.49	5.48	2.66
	Step Heating	1.82	1.39	2.02	3.78	2.35
SP3	Referred PuCT	8.42	14.67	13.67	16.40	4.60
	Step Heating	7.78	12.68	12.74	12.96	2.94

### 3. Experimental setup and specimen description

#### 3.1. Experimental setup

In order to highlight the performance of PuCT method in detecting inner defects in complex structures, a comparison between PuCT and step heating thermography [72,73] was done over various samples by using the optical thermography (OT) system depicted in Fig. 6: two halogen lamps (of each 1000 W) are selected as the light source of the system. Both lamps are located 80 cm away from the sample surface. The voltage and the current of the excitation source (ZY-B type with maximum energy of 3KW) can be adjusted. The IR camera is FLIR A655sc model with a resolution of  $640 \times 480$  and a thermal sensitivity of  $0.05^\circ\text{C}$ . The acquisition rate of the thermal camera ranges from 12.5 to 200 Hz - it was set to 50 Hz for the reported research. The IR camera and halogen lamps can be triggered synchronously by a pulse generator.

#### 3.2. Specimen description

Three specimens were used in the experiments. The specimen 1 (SP1) was a flat bottom hole specimen, which was mainly used for a verification test. The specimen 2 (SP2) and the specimen 3 (SP3) were provided by the Chengdu Aircraft Design Institute of China Aviation Industry representing actual materials used in aircraft manufacturing and production. In these samples, each ply of the carbon fibers is 0.125 mm thick. The structure of the specimens is shown in Table 1. All units are in millimeters.

SP1 has three rows of defects, and in each row the diameter of the defects is fixed. The first row has defects of 5 mm in diameter, the second row has defects of 20 mm, and the third row has defects of



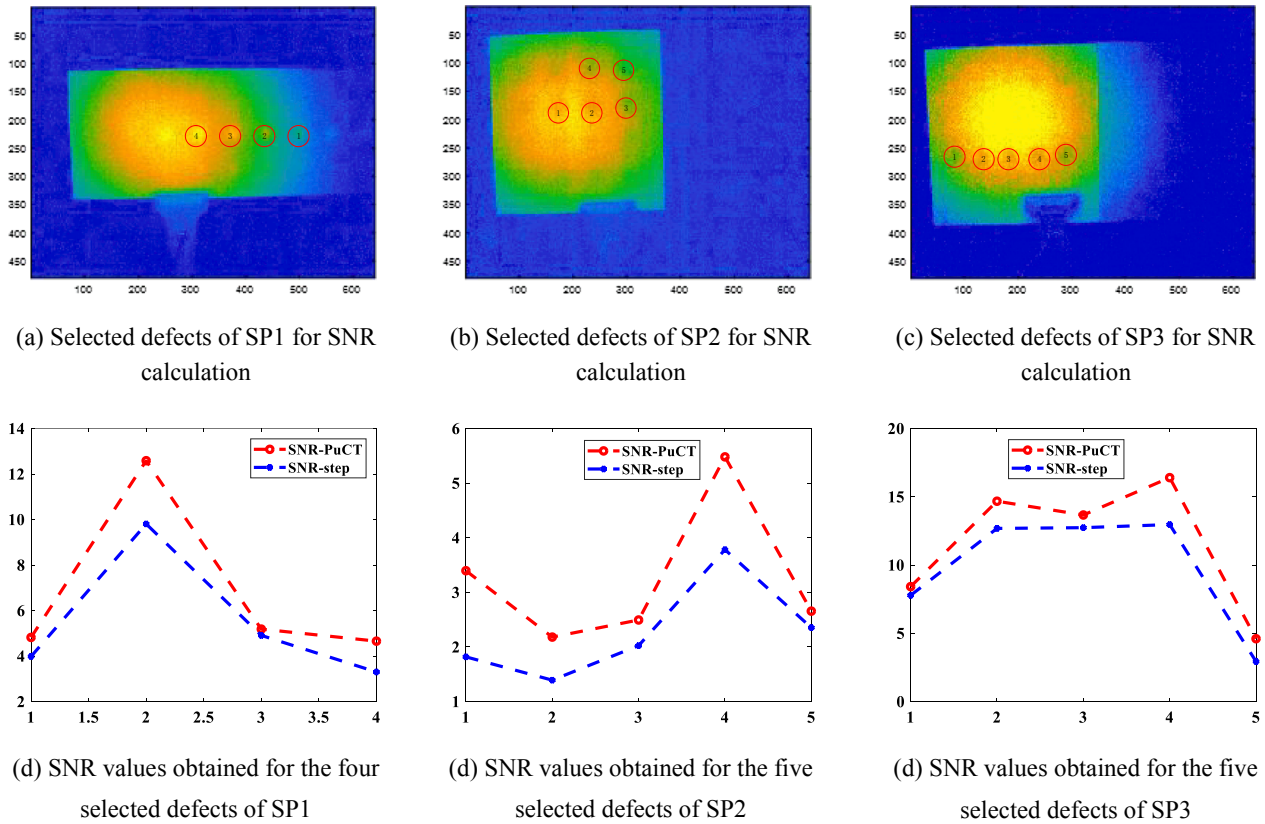


Fig. 9. The SNR of three specimens acquired by the step heating thermography and the PuCT method.

10 mm. Defects' depth gradually increases from left to right. The size and depth of the defects are shown in the table.

SP2 contains instead 16 debonding defects with different depths. Finally, the structure of SP3 is a sandwich structure consisting of external carbon fiber layers with a honeycomb inner structure. In SP3, 10 defects are located on the honeycomb structure and 10 defects are located under the honeycomb structure, as shown in the table. The thickness of the honeycomb is 10 mm, and the thickness of the rubber layer is 0.2 mm. Therefore, the front-up, front-under, rear-up, rear-under represent the defect depth of 2 mm, 2.2 mm, 12.2 mm, 12.4 mm in the sketch, respectively.

#### 4. Experiment result and analysis

As said, a comparative study was performed between step heating thermography and pulse-compression thermography. The total energy of the coded signal is the same as the total energy of the step signal. Firstly, the 13-bit Barker code was used in the samples, with a single bit duration  $T_{bit} = 300[\text{ms}]$  for SP1 and SP2. Then, a step heating thermography experiment was carried out for both samples by using a pulse duration of 1500[ms]. Because of the higher thickness of the SP3, a single-bit duration equal to 500 ms was used for the 13-bit Barker unipolar excitation while a duration of 2500[ms] was set for the step excitation. The peak power is the same in both methods.

The results of the comparison are shown in Table 2, including the best thermal images and the temperature signals in temporal domain. In the case of the 20 mm-diameter defects of SP1, step heating thermography was able to detect defects up to a depth of 3.5 mm while PuCT was able to detect defects up to 4 mm of depth. However, the SNR of the 3.5 mm defect in step heating thermography was poor. For the case of 10 mm-diameter defects, the PuCT method detected few defects, even with low contrast, while the step heating thermography method failed completely their detection. For the case of 5 mm-defects, nor the step

heating thermography neither the PuCT method were able to detect any of them. To summarize, in the case of SP1, it was found that the PuCT method can enhance the defect detection and increase the thermal contrast between the defects and the background. For SP2, the number of the detected defects was the same for both methods because of the smaller thickness of the specimen that contained just shallow defects, however PuCT defects image has a better spatial resolution than the step-heating one. For SP3, results are reported in Table 2(c) and (f). A large number of defects were detected by PuCT method than by step heating thermography: the number of the detected defects by step heating thermography is 5 while the total number of detected defects by PuCT is 8. In particular, three defects in the upper row are detected with PuCT. Although the defects of the upper row is only 0.2 mm deeper than that of the lower row, the difficulty of detection increases significantly due to the presence of the honeycomb structure. This is because the additional 0.2 mm is made of adhesive layer with poor thermal conductivity.

To further validate the comparison, the thermal contrast was calculated and compared on both step heating and PuCT images. The thermal contrast is here defined as the weighted average temperature difference between the defect and the background area. As reported in Fig. 7, we have taken 2 points, named "a" and "b", so as to calculate the thermal contrast value. Point "a" represents the pixel at the center of defect 1. We have assumed that the thermal feature of point "a" is the expected feature of the defect. Point "b" is the background near defect 1. We have taken point "a" as the center point of defect 1, selected a 7-by-7 pixels area to calculate the mean value. We have chosen point "b" as the reference for the background. The size of point "b", thus the one of the background is, is still 7-by-7 pixels. The thermal contrast is obtained by the Subtraction of the two mean value.

As shown in Fig. 8, the thermal contrast value is obtained by choosing the maximum value in time series. The defects selected in SP1, SP2 and SP3 for the calculation of the thermal contrast are marked.

Four defects were selected in SP1 and five defects in SP2 and SP3. For all the specimens, the thermal contrast obtained with PuCT is higher than that of the step heating thermography. Besides, it can be seen that the longer is the time of the single bit of Barker code, the bigger the is the thermal contrast obtained. The difference in the maximum thermal contrast obtained by the two methods is shown in Table 3. The thermal contrast results obtained by the two methods are shown in Table 4.

It can be seen from the overall data that the proposed method can effectively improve the thermal contrast. In particular, the maximum thermal contrast difference among all the defects considered is 55.34, which belongs to a defect in the SP3, while the average value of maximum contrast for defects in SP3 is 42.83. For the SP1, the maximum contrast achieved for the four defects is 28.67, with an average value equal to 21.82. The minimum thermal contrast measured is equal to 3.19 for a defect in SP2, whereas the average value of thermal contrast difference for SP2 defects is 3.85.

The results evidence the robustness of the proposed method. In addition, the thermal contrast achievable with PuCT is affected by material properties and excitation time. The longer the excitation time, the greater the difference in thermal contrast.

In addition, we have calculated the SNR (Signal to Noise Ratio) so that the results are intuitive and reliable. It is calculated as shown in Eq. (7).

$$SNR(t) = \frac{|mean_a(t) - mean_b(t)|}{std_b(t)} \quad (7)$$

The max values of SNR are shown in Table 5 and Fig. 9. It can be seen that the referred PuCT method have higher SNR values.

The results show that the proposed PuCT method with halogen lamp which remove the step heating response can effectively improve the thermal contrast and SNR of the results and detect deeper defects.

## 5. Conclusion and future work

In this paper, a PuCT protocol based on Barker code excitation and halogen lamp heating source is proposed and applied to the defect detection of carbon fiber composites. For correctly removing the step heating trend overlying the unipolar coded excitation output, and for contextually overcoming the influence of the delay characteristics of halogen lamps, experimental data acquired with a proper step heating excitation are used as background to be subtracted. The qualitative and quantitative analysis performed on experimental data allowed to demonstrated the superiority of PuCT method in defect detection with respect a step heating excitation strategy. The results show that the PuCT method can effectively suppress the noise, improve the thermal contrast, providing benefits to deeper defects detection in CFRP materials. Future work will focus on establishing a fitting curve suitable for the halogen lamp to remove the  $y_{SQ}(t)$  contribution, which simplifies the operation of PuCT method for halogen lamp without requiring a background experimental measurement.

## Declaration of Competing Interest

We declare that we do not have any commercial or associative interest that represents a conflict of interest in connection with the work submitted.

## Acknowledgement

The work was supported by Science and Technology Department of Sichuan, China (Grant No. 2019YJ0208, Grant No. 2018JY0655).

## References

- [1] W.J. Cantwell, J. Morton, The impact resistance of composite materials—a review, *Composites* 22 (5) (1991) 347–362.
- [2] K. Wang, B. Young, S.T. Smith, Mechanical properties of pultruded carbon fibre-reinforced polymer (CFRP) plates at elevated temperatures, *Eng. Struct.* 33 (7) (2011) 2154–2161.
- [3] F.P. Miller, A.F. Vandome, J. Mcbrewhster, Carbon Fiber-Reinforced Polymer, Alphascript Publishing, 2011.
- [4] G. Williams, R. Trask, I. Bond, A self-healing carbon fibre reinforced polymer for aerospace applications, *Compos. A Appl. Sci. Manuf.* 38 (6) (2007) 1525–1532.
- [5] P.D. Mangalgiri, Composite materials for aerospace applications, *Bull. Mater. Sci.* 22 (3) (1999) 657–664.
- [6] J. Guo, X. Gao, E. Toma, et al., Anisotropy in carbon fiber reinforced polymer (CFRP) and its effect on induction thermography, *NDT and E Int.* 91 (2017) 1–8.
- [7] C. IbarraCastanedo, X.P. Maldague, Review of pulsed phase thermography, *Spie Sens. Technol. Appl.* 9485 (2015) 94850T.
- [8] G. Mook, R. Lange, O. Koeser, Non-destructive characterisation of carbon-fibre-reinforced plastics by means of eddy-currents, *Compos. Sci. Technol.* 61 (6) (2001) 865–873.
- [9] F. Bastianini, A.D. Tommaso, G. Pascale, Ultrasonic non-destructive assessment of bonding defects in composite structural strengthenings, *Compos. Struct.* 53 (4) (2001) 463–467.
- [10] Vladimir P. Vavilov, Douglas D. Burleigh, Review of pulsed thermal NDT: Physical principles, theory and data processing, *NDT and E Int.* 73 (2015) 28–52.
- [11] P. Cawley, The rapid non-destructive inspection of large composite structures, *Composites* 25 (5) (1994) 351–357.
- [12] D. Hsu, V. Kommareddy, D. Barnard, et al., Aerospace Ndt using piezoceramic air-coupled transducers, *Proceedings of the 16th WCNDT*, (2004).
- [13] B. Lutz, L. Cheng, Z. Guan, L. Wang, Microwave-based detection of internal defects in composite insulators for outdoor application, 2012 IEEE International Conference on Condition Monitoring and Diagnosis, IEEE, 2012, pp. 1175–1178.
- [14] K. Koyama, H. Hoshikawa, G. Kojima, Eddy current nondestructive testing for carbon fiber-reinforced composites, *J. Pressure Vessel Technol.* 135 (4) (2013) 041501.
- [15] N.P. Avdelidis, D.P. Almond, A. Dobbins, B.C. Hawtin, C. Ibarra-Castanedo, X. Maldague, Aircraft composites assessment by means of transient thermal NDT, *Prog. Aerospace Sci.* 40 (2004) 143e62.
- [16] B.B. Lahiri, S. Bagavathiappan, P.R. Reshmi, J. Philip, T. Jayakumar, B. Raj, Quantification of defects in composites and rubber materials using active thermography, *Infrared Phys. Technol.* 35 (2e3) (2012) 191e9.
- [17] X. Li, B. Gao, et al., Periodic pulsed thermography for inner defects detection of lead-steel bonded structure, *IEEE Sens. J. PP* (99) (2018) 1.
- [18] S. Laureti, S. Sfarra, H. Malekmohammadi, P. Burrascano, D.A. Hutchins, L. Senni, M. Ricci, The use of pulse-compression thermography for detecting defects in paintings, *NDT and E Int.* 98 (2018) 147–154.
- [19] Cramer, K. Elliott, et al., Quantitative NDE of Composite Structures at NASA, 2015.
- [20] S. Bagavathiappan, B.B. Lahiri, T. Saravanan, J. Philip, T. Jayakumar, Infrared thermography for condition monitoring—A review, *Infrared Phys. Technol.* 60 (2013) 35–55.
- [21] S. Doshvarpassand, C. Wu, X. Wang, An overview of corrosion defect characterization using active infrared thermography, *Infrared Phys. Technol.* (2018).
- [22] H. Malekmohammadi, S. Laureti, P. Burrascano, M. Ricci, Comparison of optimisation strategies for the improvement of depth detection capability of Pulse-Compression Thermography, *Quant. InfraRed Thermogr. J.* (2019) 1–14.
- [23] S. Laureti, C. Colantonio, P. Burrascano, M. Melis, G. Calabrò, H. Malekmohammadi, C. Pelosi, Development of integrated innovative techniques for paintings examination: the case studies of The Resurrection of Christ attributed to Andrea Mantegna and the Crucifixion of Viterbo attributed to Michelangelo's workshop, *J. Cult. Heritage* (2019).
- [24] S. Laureti, M. Khalid Rizwan, H. Malekmohammadi, P. Burrascano, M. Natali, L. Torre, M. Ricci, Delamination detection in polymeric ablative materials using pulse-compression thermography and air-coupled ultrasound, *Sensors* 19 (9) (2019) 2198.
- [25] S. Sfarra, et al., An innovative nondestructive perspective for the prediction of the effect of environmental aging on impacted composite materials, *Int. J. Eng. Sci.* 102 (2016) 55–76.
- [26] Y. Duan, S. Huebner, U. Hassler, A. Osman, C. Ibarra-Castanedo, et al., Quantitative evaluation of optical lock-in and pulsed thermography for aluminum foam material, *Infrared Phys. Technol.* 60 (5) (2013) 275–280.
- [27] A. Foudazi, K.M. Donnell, M.T. Ghasr, Application of active microwave thermography to delamination detection, 2014 IEEE International Instrumentation and Measurement Technology Conference (I2MTC) Proceedings, IEEE, 2014, pp. 1567–1571.
- [28] G.P.M. Fierro, D. Ginzburg, F. Ciampa, M. Meo, Nonlinear ultrasonic stimulated thermography for damage assessment in isotropic fatigued structures, *J. Sound Vib.* 404 (2017) 102–115.
- [29] M.C. Di Tuccio, N. Ludwig, M. Gargano, A. Bernardi, Thermographic inspection of cracks in the mixed materials statue: Ratto delle Sabine, *Herit. Sci.* 3 (1) (2015) 10.

- [30] C. Ibarra-Castaneda, S. Sfarra, D. Ambrosini, D. Paoletti, A. Bendada, X. Maldague, Diagnostics of panel paintings using holographic interferometry and pulsed thermography, *Quant. InfraRed Thermogr. J.* 7 (1) (2010) 85–114.
- [31] L. Cheng, G.Y. Tian, Surface crack detection for carbon fiber reinforced plastic (CFRP) materials using pulsed eddy current thermography, *IEEE Sens. J.* 11 (12) (2011) 3261–3268.
- [32] Q. Yi, G.Y. Tian, H. Malekmohammadi, J. Zhu, S. Laureti, M. Ricci, New features for delamination depth evaluation in carbon fiber reinforced plastic materials using eddy current pulse-compression thermography, *NDT and E Int.* 102 (2019) 264–273.
- [33] A O Chulkov, V P Vavilov, Hardware and software for thermal nondestructive testing of metallic and composite materials, *J. Phys.: Conf. Ser.* 671 (2016) 012011, <https://doi.org/10.1088/1742-6596/671/1/012011>.
- [34] F. Mabrouki, M. Genest, G. Shi, A. Fahr, Numerical modeling for thermographic inspection of fiber metal laminates, *NDT and E Int.* 42 (2009) 581–588.
- [35] H. Fernandes, H. Zhang, A. Figueiredo, et al., Carbon fiber composites inspection and defect characterization using active infrared thermography: numerical simulations and experimental results, *Appl. Opt.* 55 (34) (2016) D46.
- [36] Y. Liu, Q. Tang, C. Bu, et al., Pulsed infrared thermography processing and defects edge detection using FCA and ACA, *Infrared Phys. Technol.* 72 (2015) 90–94.
- [37] N.P. Avdelidis, B.C. Hawtin, D.P. Almond, Transient thermography in the assessment of defects of aircraft composites, *NDT and E Int.* 36 (2003) 433–439.
- [38] F. Qizhi, G. Bin, L. Peng, et al., Automatic seeded region growing for thermography debonding detection of CFRP, *NDT and E Int.* 99 (2018) 36–49.
- [39] J.A. Schroeder, T. Ahmed, B. Chaudhry, S. Shepard, Non-destructive testing of structural composites and adhesively bonded composite joints: pulsed thermography, *Compos. A Appl. Sci. Manuf.* 33 (2002) 1511–1517.
- [40] X. Maldague, S. Marinetti, Pulse phase infrared thermography, *J. Appl. Phys.* 79 (5) (1996) 2694–2698.
- [41] C. Meola, G.M. Carlomagno, A. Squillace, A. Vitiello, Non-destructive evaluation of aerospace materials with lock-in thermography, *Eng. Fail. Anal.* 13 (3) (2006) 380–388.
- [42] D. Wu, G. Busse, Lock-in thermography for nondestructive evaluation of materials, *Revue Générale De Thermique* 37 (1998) 693–703.
- [43] T. Sakagami, S. Kubo, Applications of pulse heating thermography and lock-in thermography to quantitative nondestructive evaluations, *Infrared Phys. Technol.* 43 (2002) 211–218.
- [44] S. Pickering, D. Almond, Matched excitation energy comparison of the pulse and lock-in thermography NDE techniques, *NDT and E Int.* 41 (2008) 501–509.
- [45] K. Chatterjee, S. Tuli, S.G. Pickering, D.P. Almond, A comparison of the pulsed, lock-in and frequency modulated thermography nondestructive evaluation techniques, *NDT and E Int.* 44 (7) (2011) 655–667.
- [46] Przemysław Daniel Pastuszek, Characterization of defects in curved composite structures using active infrared thermography ☆, *Procedia Eng.* 157 (2016) 325–332.
- [47] C.A. Alvarez-Restrepo, H.D. Benitez-Restrepo, L.E. Tobón, Characterization of defects of pulsed thermography inspections by orthogonal polynomial decomposition, *NDT and E Int.* 91 (2017) 9–21.
- [48] R. Mulaveesala, S. Tuli, Theory of frequency modulated thermal wave imaging for nondestructive subsurface defect detection, *Appl. Phys. Lett.* 89 (2006).
- [49] V.S. Ghali, N. Jonnalagadda, R. Mulaveesala, Three-dimensional pulse compression for infrared nondestructive testing, *IEEE Sens. J.* 9 (7) (2009) 832–833.
- [50] N. Tabatabaei, A. Mandelis, Thermal-wave radar: a novel subsurface imaging modality with extended depth-resolution dynamic range, *Rev. Sci. Instrum.* 80 (3) (2009) 034902.
- [51] I. Mohamed, D. Hutchins, L. Davis, S. Laureti, M. Ricci, Ultrasonic NDE of thick polyurethane flexible riser stiffener material, *Nondestruct. Test. Evaluat.* 32 (4) (2017) 343–362.
- [52] D. Hutchins, P. Burrascano, L. Davis, S. Laureti, M. Ricci, Coded waveforms for optimised air-coupled ultrasonic nondestructive evaluation, *Ultrasonics* 54 (7) (2014) 1745–1759.
- [53] S. Harput, J. McLaughlan, D.M. Cowell, S. Freear, Superharmonic imaging with chirp coded excitation: filtering spectrally overlapped harmonics, *IEEE Trans. Ultrason. Ferroelectr. Freq. Control* 61 (11) (2014) 1802–1814.
- [54] N. Tabatabaei, A. Mandelis, Thermal coherence tomography using match filter binary phase coded diffusion waves, *Phys. Rev. Lett.* 107 (2011) 1–5.
- [55] S. Kaipilavil, A. Mandelis, Highly depth-resolved chirped pulse photothermal radar for bone diagnostics, *Rev. Sci. Instrum.* 82 (2011) 29.
- [56] V.S. Ghali, S.S.B. Panda, R. Mulaveesala, Barker coded thermal wave imaging for defect detection in carbon fibre-reinforced plastics, *Insight - Non-Destruct. Test. Cond. Monit.* 53 (53) (2011) 621–624.
- [57] Giuseppe Silipigni, Pietro Burrascano, David A. Hutchins, Stefano Laureti, Roberto Petrucci, Luca Senni, Luigi Torre, Marco Ricci, Optimization of the pulse-compression technique applied to the infrared thermography nondestructive evaluation, *NDT and E Int.* 87 (2017) 100–110, <https://doi.org/10.1016/j.ndteint.2017.01.011>.
- [58] V. Arora, R. Mulaveesala, P. Bison, Effect of spectral reshaping on frequency modulated thermal wave imaging for non-destructive testing and evaluation of steel material, *J. Nondestruct. Eval.* 35 (1) (2016) 1–7.
- [59] S. Laureti, G. Silipigni, L. Senni, R. Tomasello, P. Burrascano, M. Ricci, Comparative study between linear and non-linear frequency-modulated pulse-compression thermography, *Appl. Opt.* 57 (18) (2018) D32–D39.
- [60] A.V. Lakshmi, V. Gopitilak, M.M. Parvez, S.K. Subhani, V.S. Ghali, Artificial neural networks based quantitative evaluation of subsurface anomalies in quadratic frequency modulated thermal wave imaging, *Infrared Phys. Technol.* 97 (2019) 108–115.
- [61] B. Suresh, S.K. Subhani, A. Vijayalakshmi, V.H. Vardhan, V.S. Ghali, Chirp Z transform based enhanced frequency resolution for depth resolvable non stationary thermal wave imaging, *Rev. Sci. Instrum.* 88 (1) (2017) 014901.
- [62] C. Meola, Nondestructive evaluation of materials with rear heating lock-in thermography, *IEEE Sens. J.* 7 (10) (2007) 1388–1389.
- [63] Krishnendu Chatterjee, Deboshree Roy, Suneet Tuli, A novel pulse compression algorithm for frequency modulated active thermography using bandpass filter, *Infrared Phys. Technol.* 82 (2017) 75–84.
- [64] Deboshree Roy, Suneet Tuli, Applicability of LED-based excitation source for defect depth resolved frequency modulated thermalwave imaging, *IEEE Trans. Instr. Measur.* 66 (10) (2017) 2658–2665.
- [65] T. Misaridis, J.A. Jensen, Use of modulated excitation signals in medical ultrasound. Part I: basic concepts and expected benefits, *IEEE Trans. Ultrason., Ferroelectr., Freq. Control* 52 (2) (2005) 177–191.
- [66] P. Burrascano, S. Laureti, L. Senni, M. Ricci, Pulse compression in nondestructive testing applications: reduction of near sidelobes exploiting reactance transformation, *IEEE Trans. Circuits Syst. I Regul. Pap.* 99 (2018) 1–11.
- [67] L. Lei, G. Ferrarini, A. Bortolin, G. Cadelano, P. Bison, X. Maldague, Thermography is cool: defect detection using liquid nitrogen as a stimulus, *NDT and E Int.* 102 (2019) 137–143.
- [68] Nadav Levanon, Noncoherent pulse compression, *IEEE Trans. Aerosp. Electron. Syst.* 42 (2) (2006) 756–765.
- [69] R. Oslander, J.W. Spicer, Time-resolved infrared radiometry with step heating. A review, *Revue Générale de Thermique* 37 (8) (1998) 680–692.
- [70] J.M. Spicer, W.D. Kerns, L.C. Aamodt, J.C. Murphy, Measurement of coating physical properties and detection of coating disbands by time-resolved infrared radiometry, *J. Nondestruct. Eval.* 8 (2) (1989) 107–120.
- [71] J.M. Spicer, W.D. Kerns, L.C. Aamodt, J.C. Murphy, Time-resolved infrared radiometry (TRIR) for characterization of impact damage in composite materials, *Review of Progress in Quantitative Nondestructive Evaluation*, Springer, Boston, MA, 1992, pp. 433–440.
- [72] D.P. Almond, S.L. Angioni, S.G. Pickering, Long pulse excitation thermographic non-destructive evaluation, *NDT and E Int.* 87 (2017) 7–14.
- [73] Z. Wang, G. Tian, M. Meo, F. Ciampa, Image processing based quantitative damage evaluation in composites with long pulse thermography, *NDT and E Int.* 99 (2018) 93–104.